Dimeric prion protein ligand activates Adgrg6 but does not rescue myelinopathy of PrP-deficient mice

Abbreviated title: Adgrg6 activation by PrP

Anna Henzi[1§], Assunta Senatore[1], Asvin KK Lakkaraju[1], Claudia Scheckel[1], Jonas Mühle[2], Regina Reimann[1], Silvia Sorce[1], Gebhard Schertler[2], Klaus V Toyka[3], Adriano Aguzzi[1§]

[1] Institute of Neuropathology, University of Zurich, Schmelzbergstrasse 12, 8091 Zurich, Switzerland

[2] Paul Scherrer Institute, Forschungsstrasse 111, 5232 Villingen PSI, Switzerland

[3] Department of Neurology, University Hospital of Würzburg, University of Würzburg, Josef-Schneider-Strasse 11, 97080 Würzburg, Germany

[§]Corresponding authors: Adriano Aguzzi and Anna Henzi

e-mail: adriano.aguzzi@usz.ch, anna.henzi@usz.ch

Submitting author: Anna Henzi

Keywords: Adhesion G-protein coupled receptor; Demyelination; Fc-fusion protein; Prion protein, Therapy, Peripheral nervous system

Summary blurb: A dimeric prion protein ligand activates Adgrg6 but fails to induce pro-myelination signaling upon chronic treatment in a mouse model of peripheral demyelination.

Abstract

The adhesion G-protein coupled receptor Adgrg6 (formerly Gpr126) is instrumental in the development, maintenance and repair of peripheral nervous system myelin. The prion protein (PrP) is a potent activator of Adgrg6 and could be used as a potential therapeutic agent in treating peripheral demyelinating and dysmyelinating diseases. We designed a dimeric Fc-fusion protein comprising the myelinotrophic domain of PrP (FT_2Fc), which activated Adgrg6 in vitro and exhibited favorable pharmacokinetic properties for in vivo treatment of peripheral neuropathies. While chronic FT_2Fc treatment elicited specific transcriptomic changes in the sciatic nerves of PrP knockout mice, no amelioration of the peripheral demyelinating neuropathy was detected. Instead, RNA sequencing of sciatic nerves revealed downregulation of cytoskeletal and sarcomere genes, akin to the gene expression changes seen in myopathic skeletal muscle of PrP overexpressing mice. These results call for caution when devising myelinotrophic therapies based on PrP-derived Adgrg6 ligands. While our treatment approach was not successful, Adgrg6 remains an attractive therapeutic target to be addressed in other disease models or by using different biologically active Adgrg6 ligands.

Introduction

The prion protein (PrP), encoded by the *PRNP* gene, is mainly known for its role as the causative infectious agent in prion diseases, a group of fatal neurodegenerative diseases. Yet the remarkable evolutionary conservation of PrP suggests that it exerts physiological functions. Mice ablated for PrP (Nishida et al., 1999; Bremer et al., 2010) and goats lacking PrP due to a naturally occurring mutation (Skedsmo et al., 2020) develop a progressive peripheral demyelinating neuropathy, indicating that PrP is involved in myelin maintenance. Although no mutations in the human *PRNP* gene were found in a study of patients with hereditary neuropathies (Koop et al., 2005), the alteration of PrP or its sequestration in aggregates could explain the development of peripheral neuropathy in patients suffering from Creutzfeldt-Jakob disease (Baiardi et al., 2019). This notion is supported by the occurrence of pronounced peripheral demyelination in certain genetic forms of Creutzfeldt-Jakob disease (Neufeld et al., 1992). Moreover, a patient with two pathogenic *PRNP* mutations was reported to develop an early onset peripheral demyelinating neuropathy (Piazza et al., 2020).

The mechanism by which PrP exerts its function in myelin maintenance has recently been identified (Kuffer et al., 2016). The N-terminal fragment, termed flexible tail (FT), comprises the myelinotrophic domain of PrP. FT is released by proteolysis and activates the adhesion G-protein coupled receptor Adgrgr6 on Schwann cells. Both in vitro and in vivo, activation of Adgrg6 by a peptide derived from FT results in cAMP accumulation and promyelinating signaling. In the peripheral nervous system (PNS), Adgrg6 is crucial for the development of the myelin sheath in zebrafish (Monk et al., 2009) and mice (Monk et al., 2011). In addition, Adgrg6 is involved in the remyelination of axons (Mogha et al., 2016) and reinnervation of neuromuscular junctions (Jablonka-Shariff et al., 2020) after nerve injury. Whereas the inducible knockout of Adgrg6 in Schwann cells did not result in signs of demyelination for up to 4 months (Mogha et al., 2016), aged conditional Adgrg6 knockout mice showed neuromuscular junction alterations and signs of denervation in hindlimbs, consistent with chronic disruption of Schwann cell function (Jablonka-Shariff et al., 2020). Together with the

late-onset demyelinating neuropathy of PrP knockout mice, these findings suggest that Adgrg6 is not only required for the initiation of myelination, but also for long-term myelin maintenance.

The role of Adgrg6 in myelination and remyelination suggests that it could be a promising therapeutic target for peripheral demyelinating diseases and possibly other diseases linked to Adgrg6 malfunction, such as adolescent idiopathic scoliosis (Xu et al., 2019). We therefore set out to explore the therapeutic potential of stimulating Adgrg6-dependent promyelinating pathways using its natural ligand PrP. To this end, we constructed a dimeric fusion protein consisting of the FT linked to crystallizable fragment (Fc) of immunoglobulin G1 (FT_2Fc). FT_2Fc showed favorable pharmacokinetic properties in vivo including a half-life of 45 h but failed to have a therapeutic effect on the demyelinating neuropathy in PrP knockout mice. Instead, gene expression analysis of sciatic nerves from mice treated with FT_2Fc revealed unexpected changes in cytoskeletal and contractile elements. The observed transcriptomic changes were similar to the changes elicited by PrP overexpression in skeletal muscle, which causes a necrotizing myopathy (Westaway et al., 1994; Huang et al., 2007).

Material and methods

Mice

Breeding and maintenance of mice was performed in specified-pathogen-free facilities at the University Hospital Zurich. Mice were housed in groups of 3–5, under a 12 h light/12 h dark cycle, with sterilized chow food and water *ad libitum*. The protocols for animal care and experiments were in accordance with the Swiss Animal Protection Law. All experiments were approved by the Veterinary Office of the Canton of Zurich (permits ZH139/2016 and ZH201/2018). For experiments with FT_2Fc, male and female C57BL/6J (WT) and PrP knockout (ZH3) mice were used. Mice were intravenously or intraperitoneally injected with various dosages of FT_2Fc, mIgG (5-10 mg/Kg bodyweight), sodium phosphate buffer (20 mM, pH 7), FT or control peptide. Blood samples were collected from the saphenous vein and serum was obtained by centrifugation of clotted blood for 1.5 min at 10'000 g. For the pharmacokinetic studies and acute treatment experiment, adult mice were used. Chronic treatment was started at 1 month of age and lasted for 4 months.

Transgenic mice expressing tamoxifen-inducible Cre under the control of the human ACTA1 (Actin, alpha 1, skeletal muscle) promoter were bred with mice expressing loxP-flanked *Prnp* (C57BL/6J-Tg(CAG-cat,-Prnp)56Aag x Tg(ACTA1-cre/Esr1*)2Kesr/J) to achieve tamoxifen-inducible PrP overexpression in skeletal muscle. Mice were given food pellets with 400 mg/kg tamoxifen (Envigo) for one week to induce Cre-recombination. Male mice were sacrificed for organ collection 14 days after induction. CAG+/Cre+ mice were compared to CAG+/Cre-, CAG-/Cre- and CAG-/Cre- mice.

Electrophysiological investigations

Electrophysiological investigations were performed on the sciatic nerve of mice treated with FT_2Fc or control treatment. Mice were anesthetized with Ketamine-Xylazine and electrophysiological investigations were performed as previously described (Zielasek et al., 1996; Gerber et al., 2019). The investigators were blinded as to the treatment and strain of the mice during the tests as well as post-hoc analyses.

Morphological analysis

For toluidine blue stained sections, sciatic nerves were dissected and incubated in 4% glutaraldehyde in 0.1 M sodium phosphate buffer pH 7.4 at 4 °C overnight. Tissue was embedded in Epon using standard procedures and semithin sections (500 nm) were stained with toluidine blue. Counting of myelinated axons was performed manually on one 313 x 197 µM field of view per mouse with the observer blinded as to the treatment group. Then number of myelinated axons was normalized to the area. For cryosections of gastrocnemius muscle, the tissue was frozen in Optimal Cutting Temperature compound using liquid nitrogen and cut in 10 µM sections at the cryostat. Slides were incubated in 4% paraformaldehyde for 10 min and washed three times in PBS. The sections were first incubated in hematoxylin for 10 min, and then in trichrome staining solution (Chromotrope 2R 0.6% w/v (Chroma 1B259), fast green FCF 0.3% w/v (BDH 340304F), phosphotungstic acid 0.6 % w/v, acetic acid 0.5 %, pH 3.4) for 20 min. Finally, the sections were incubated in 0.5% acetic acid for differentiation and dehydrated in ethanol.

Cell culture

Wild type SW10 cells and SW10 cells devoid of Adgrg6 were grown in DMEM (Gibco) supplemented with 10% FBS, penicillin-streptomycin and glutamax (Invitrogen) at 33 °C. FreeStyle™ 293-F (Thermofisher, R790-07) cells were grown in FreeStyle medium (Thermofisher, 12338018) on an orbital shaker (140 rpm) at 37 °C.

Transfection

The mammalian expression vector for FT_2Fc was obtained from ATUM (vector pD2610-v1). 293-F cells were seeded 2-3 h before transfection at a density of $1x10^6$ cells per ml in Freestyle medium supplemented with 0.2% w/v HyClone Cell Boost (GE Healthcare, SH30584.02). For transient transfection, 1 µg of plasmid and 2 µl of 40 kD linear polyethyleneimine (1 mg/ml, Polysciences, 24765-1) were used per milliliter of cells. For protein production, cells were supplemented with 2% w/v HyClone every 2-3 days (10% of culture volume each time). At 7 days post transfection, cell culture supernatant was cleared by centrifugation at 2'500 g for 10

138 min at 4 °C. The medium was sterile filtered and stored at 4 °C or –20 °C until further
139 processing.

140 *Protein purification*

141 Cell culture supernatant was diluted 1:1 in binding buffer (0.16 M sodium phosphate, 500 mM
142 NaCl, pH 9) and loaded on a Protein A Sepharose (Sigma Aldrich, 17-1279-03) column at a
143 flow rate of 2 ml/min. After washing with 5 column volumes of binding buffer until a stable
144 baseline was reached, FT_2Fc was eluted with elution buffer (0.1 M sodium citrate, pH 2.7). 500
145 µl fractions were collected and immediately neutralized with 50 µl 1 M Tris/HCl, pH 8. Elution
146 fractions were analyzed by 12% or gradient 4-12% NuPAGE Bis-Tris gels (Invitrogen) followed
147 by Coomassie staining. Fractions containing purified protein were pooled and dialyzed
148 overnight against storage buffer (0.02 M sodium phosphate, pH 7) in a 10 kD cut off dialysis
149 cassette (ThermoFisher, 66380). Purified protein was stored at 4 °C for use within days or at
150 –20 °C for longer-term storage.

151 *RNA extraction, library preparation and sequencing*

152 For sciatic nerves, total RNA was extracted using TRIzol (Invitrogen Life Technologies, 15596-
153 018) according to the manufacturer's instructions. The phenol-chloroform phase was
154 subsequently used for protein extraction. For RNA extraction of tibialis muscle from PrP
155 overexpressing mice, the tissue was snap-frozen in liquid nitrogen and ground using the
156 CryoGrinder™ kit system following the manufacturer's instructions. The RNA was extracted
157 using the RNeasy Plus Universal Kit (Qiagen). Library preparation, RNA sequencing and
158 bioinformatic analysis were performed at the Functional Genomics Center Zurich (FGCZ). For
159 sciatic nerves of untreated 4 months old mice and tibialis muscle of PrP overexpressing mice,
160 library preparation and RNA sequencing were performed as described previously (Sorce et al.,
161 2020). For mice in the chronic treatment experiment and 13-15 months untreated old mice,
162 libraries were prepared using the TruSeq RNA stranded Library Prep Kit (Illumina, Inc) and
163 sequencing was performed on the Illumina Novaseq 6000 instrument for single-end 100 bp
164 reads.

RNA sequencing data analysis

For all samples, quality of reads was checked with FastQC. Reads were aligned to the GRCm38 genome assembly with Ensembl gene annotations with STAR (Dobin et al., 2013). Reads were counted with the featureCounts (Liao et al., 2014) function from the R package Rsubread. Differential expression analysis was performed with the R package EdgeR (Robinson et al., 2010), using a generalized linear model with Trimmed Means of M-values (TMM) normalization. In the group pair-wise comparisons, we considered only genes with at least 10 raw counts in at least 50% of the samples in one of the groups. Genes with false discovery rate (FDR) below 0.05 were defined as differentially expressed. For the clustering analysis, the hclust function from the stats package was used. Visualizations were generated with the Sushi data analysis framework (Hatakeyama et al., 2016) provided by FGCZ or with R (version 3.5.2).

Western blot analysis

SW10 cells were lysed in ice-cold lysis buffer (phosSTOP (Sigma, 4906845001) and protease inhibitor (Sigma, 11836153001) in RIPA buffer). Sciatic nerves were homogenized in lysis buffer using stainless steel beads. The lysates were centrifuged for 10 min at 10'000 g to remove debris. Protein concentration was measured with BCA assay (Thermo Scientific) and equal amounts of protein for each sample (10-30 µg) were boiled in 4 x LDS (Invitrogen) at 95 °C for 5 min. Mouse serum was diluted 1:10 in PBS and boiled in 4 x LDS with 0.1 M dithiothreitol (DTT) for western blotting. The samples were loaded on 12% or gradient 4-12% NuPAGE Bis-Tris gels (Invitrogen). Electrophoresis was performed at 200 V. Gels were transferred to PVDF membranes with the iBlot system (Life Technologies). Membranes were blocked with 5% non-fat milk in PBS-T (for Fab83 staining) or 5% SureBlock (LuBioScience GmbH, SB232010) in TBS-T for all other staining. Then, membranes were incubated over night at 4 °C with the primary antibody diluted in blocking buffer. After three washes for 10 min, membranes were incubated with secondary antibodies coupled to horseradish peroxidase for 1 h at room temperature (RT). After washing, membranes were developed with Crescendo

chemiluminescence substrate system (Sigma, WBLUR0500) and signals were detected using a Fusion Solo S imaging system (Vilber). Densitometry was performed using the FusionCapt Advance software. Dashed lines indicate removal of irrelevant lanes by image splicing from single blots. Original, uncropped images are shown in supplementary figures S1-S4.

The following primary antibodies were used for western blotting: phospho-AKT (1:1000, Cell Signaling Technologies, 4060S), AKT (1:1000, Cell Signaling Technologies, 4685S), GFAP (1:2000, Cell Signaling Technologies, 12389S), c-Jun (1:1000, 9165s), Egr2 (1:2000, Abcam, ab108399), Calnexin (1:2000, Enzo, ADI-SPA-865-D), Actin (1:10'000, Milipore, MAB1501R). In addition, we used an in-house produced Fab-fragment directed against the N-terminus of PrP (Senatore et al., 2020) (Fab83, 6 µg/ml). The following horseradish peroxidase coupled secondary antibodies were used: anti-mouse IgG (1:10'000, Jackson Immuno Research, 115-035-003), anti-rabbit IgG (1:4000, Jackson Immuno Research, 111-035-003), anti-human Fab (1:7000, Sigma, A0293).

Enzyme-linked immunosorbent assay (ELISA)

384-well plates were coated with Fab83 (150 nM) or equimolar amount of BSA in PBS-T overnight at 4 °C. After three washes with PBS-T, plates were blocked with superblock (Thermofisher, 37515) for 2 h at RT. Next, a serial dilution of cell culture supernatant from transfected cells was incubated for 2 h at RT. After washing, goat anti-mouse IgG antibodies coupled to horseradish peroxidase (1:1000, Jackson Immuno Research, 115-035-003) were added for 1 h. Then, the plates were washed and developed with TMB (Invitrogen, SB02). The reaction was stopped with 0.5 M H_2SO_4 and absorbance at 450 nm was measured in a plate reader (Perkin Elmer, EnVision). The experiment was performed with technical duplicates.

Immunoprecipitation

Immunoprecipitation (IP) of FT_2Fc from cell culture supernatant was performed as previously described with minor modifications (Senatore et al., 2020). Briefly, sheep-anti mouse IgG paramagnetic beads (Dynal, 11201D) were coupled with anti-His mAb (Invitrogen, 37-2900) in coating buffer (PBS plus 0.1% immunoglobulin-free BSA) for 2 h at RT on a rotating wheel.

Three molar excess of His-tagged Fab83 were added. After 1 h incubation, beads were washed three times with coating buffer. Cell culture supernatant was diluted 1:1 in IP buffer (50 mM Tris-Cl, 75 nM NaCl, 1% Igepal, protease inhibitor mixture (Sigma, 11836153001), pH 7.4) plus 0.5% BSA and incubated with 50 µl of Fab83-anti-His antibody coupled beads. The same input was used for all conditions. IP was performed overnight at 4 °C. After five washes with 50 mM Tris-Cl, 0.5% Igepal, 150 nM NaCl, 0.5% BSA, pH 7.4, elution of immunoprecipitated FT_2Fc was performed by incubation with peptides (200 molar excess compared to Fab83) for 2 h at 4 °C. The eluate was boiled in 4 x LDS for western blotting. After elution, the beads were boiled in 4 x LDS and the supernatant was investigated by western blotting.

Thermal shift assay

FT_2Fc (1 µg) was diluted in 20 µl of 20 mM sodium phosphate, pH 7, with a final concentration of 10x SYPRO orange (Sigma, S5692). The temperature was increased from 25 °C to 95 °C at 3 °C per minute and fluorescence was measured at 610 nm in a Rotor-Gene Q thermocycler (Qiagen). The experiment was performed in technical triplicates. The fluorescence-temperature curves were fitted to the Boltzmann equation using GraphPad Prism (version 8.4.2) to determine the inflection point, which corresponds to the melting temperature.

cAMP measurements

cAMP levels were measured as previously described (Kuffer et al., 2016) using a colorimetric competitive immunoassay (Enzo Life Sciences). Briefly, SW10 cells were plated in 6-well plates to ~50% density. Cells were incubated with FT_2Fc, FT or control treatment for 20 min and then lysed with 0.1 M HCl buffer for 20 min. The lysate was cleared by centrifugation at 600 g for 10 min and then processed according to the manufacturer's protocol.

Experimental design and statistical analysis

GraphPad Prism software (version 8.4.2) was used for statistical analysis and data processing except for RNA sequencing data analysis. Normal distribution and equal variances of data

were assumed, but this was not formally tested due to small *n* values. For the chronic treatment study, the sample size was determined with a power calculation based on the results from our previous electrophysiological studies (Bremer et al., 2010): at least 10 mice per group were required to detect a 6 m/s difference in motor nerve conduction velocity between treatment groups assuming a standard deviation of 4.4 m/s (power 90%, type I error 5%). For all other experiments, sample sizes were chosen according to sample sizes generally used in the field. For curve fitting, we used four-parameter logistic regression analysis or nonlinear least-squares analysis as indicated in the figure legends. As a measure for the goodness of fit we reported R^2 for nonlinear regression as computed by GraphPad Prism. Comparisons of two groups were performed by unpaired or paired two-tailed t-test as indicated. For comparison of three or more groups, one- or two-way ANOVA followed by multiple comparison tests were used and p-values were reported as multiplicity adjusted p-values. We used Sidak's multiple comparison test for comparison of preselected independent pairs, Bonferroni's multiple comparisons test when the assumption of independence could not be supported, and Dunnett's method for comparison of multiple groups to one control group. P-values < 0.05 were considered statistically significant. P-values are indicated in graphs as *: $p < 0.05$, **: $p = 0.01$-0.05, ***: $p = 0.001$-0.01, ****: $p < 0.0001$. ns = not significant, $p > 0.05$. Error bars in graphs show SEM. For in vitro experiments, individual points in the graphs correspond to independent experiments (cAMP assay, pAKT analysis) or technical replicates (ELISA, thermal shift assay). For animal experiments, each lane in the western blots and each point in the graphs corresponds to one mouse unless otherwise noted. For sciatic nerve protein analysis of chronically treated mice, one FT_2Fc treated ZH3 mouse was excluded due a technical error in sample preparation. Otherwise, no samples or data were omitted during the analyses.

Data availability

The raw data from the RNA sequencing experiments will be deposited on the GEO database after publication of this study. Other data that support the findings of this study are available upon reasonable request from the corresponding author, AA.

Results

Generation of a PrP-Fc-fusion protein

The binding of FT to Adgrg6 leads to intracellular accumulation of cAMP, which is essential in driving the synthesis of proteins and lipids critical for myelin generation and maintenance (Jessen et al., 1991). We sought to investigate if sustained treatment with FT would suffice to constitutively activate Adgrg6 and thereby restore the reduced promyelination signaling in *Prnp* ablated mice (ZH3). Peptides are expected to have a short half-life in vivo, limiting their exposure to the target tissue. A common strategy to prolong the half-life of peptides is the fusion to larger molecules such as Fc (Craik et al., 2013). We generated a mammalian expression plasmid containing FT (amino acids 1-50 of mouse PrP) fused with mouse IgG1-Fc at the hinge region, which upon transfection in cells leads to the expression of the homodimeric fusion protein, FT_2Fc (Fig. 1a). The first 22 residues of FT comprise the signal peptide directing FT_2Fc for secretion, whereas residues 23-50 activate Adgrg6 (Kuffer et al., 2016). Murine IgG1-Fc is unlikely to induce inadvertent activation of the immune system, since the murine IgG1 subclass binds to the inhibitory Fcγ-receptor and does not fix complement (Collins, 2016).

To assess whether FT_2Fc is correctly assembled and secreted, we transiently transfected FreeStyle 293-F cells with the plasmid expressing FT_2Fc, resulting in secretion of FT_2Fc into the culture medium. Under non-reducing conditions FT_2Fc predominantly existed as a dimer (56 kD), whereas in the presence of reducing agents (DTT) it migrated as a monomer (Fig. 1b). We confirmed the identity of the secreted protein by western blotting using either anti-mouse IgG antibodies or a monomeric antibody Fab fragment specifically targeting the KKRPK domain of FT (Senatore et al., 2020) (Fab83). Both antibodies detected FT_2Fc in cell culture supernatant as well as purified FT_2Fc (Fig. 1b). To confirm the presence of FT_2Fc by additional methods, we performed a sandwich ELISA by capturing FT_2Fc with Fab83 and detecting the complex using anti-mouse IgG antibodies. A serial dilution of cell culture supernatant containing FT_2Fc resulted in a sigmoidal curve, whereas no signal was detected in medium

from cells transfected with the empty vector (Fig. 1c). Finally, we immunoprecipitated FT_2Fc from cell culture supernatant using beads coupled with Fab83. Peptides derived from the linear sequence of mouse PrP were previously used to map the epitope of Fab83 (Senatore et al., 2020). FT_2Fc could be eluted from the beads with a peptide competing for the Fab83 binding site (amino acids 23-34 of mouse PrP), but not with a non-competing peptide (amino acids 53-64) (Fig. 1d).

Collectively, these results suggest that a correctly assembled FT_2Fc fusion protein was secreted by 293-F cells. We purified FT_2Fc from cell culture supernatant by protein A chromatography. The melting temperature of FT_2Fc as assessed by thermal shift assay was 74.5 °C at pH 7 (Fig. 1e), which is similar to the melting temperature of other purified Fc fragments previously reported (Wozniak-Knopp et al., 2012; Dashivets et al., 2015) and implies high thermal stability of FT_2Fc during storage and handling.

FT_2Fc activates Adgrg6 signaling in vitro

cAMP signaling is involved in various steps of Schwann cell development (Jessen et al., 1991) and is required for maintenance of a differentiated state (Monje et al., 2010). Adgrg6 signals via cAMP and protein kinase A to initiate myelination in the PNS (Mogha et al., 2013). PI3K/AKT-signaling is another pathway involved in myelination and repair (Boerboom et al., 2017). A link between cAMP and AKT activation has been suggested in vitro (Monje et al., 2006). Activation of Adgrg6 by FT has previously been shown to induce cAMP signaling in primary Schwann cells, an immortalized Schwann cell line (SW10) and in vivo (Kuffer et al., 2016). In addition, phosphorylation of AKT has been demonstrated in SW10 cells upon FT treatment (Kuffer et al., 2016).

We investigated whether purified FT_2Fc can act as a ligand for Adgrg6 in vitro. SW10 cells were incubated for 20 min with equinormal (half-equimolar where appropriate because of bivalency) amounts of either FT_2Fc (2.5 µM) or FT (amino acids 23-50 of mouse PrP, 5 µM). cAMP levels in the cell lysates were measured by ELISA as previously established (Kuffer et al., 2016). Treatment of wild type SW10 cells ($SW10_{WT}$) with FT_2Fc resulted in a significant

increase in the levels of cAMP, similar to that of FT treated cells. The increase in cAMP was not observed in Adgrg6-ablated cells ($SW10_{\Delta Adgrg6}$) (Fig. 2a). When treated with increasing doses of FT_2Fc, $SW10_{WT}$ cells showed a concentration-dependent increase in cAMP levels up to a maximum 9-fold increase at 7 µM (Fig. 2b). Nonlinear regression analysis revealed an EC_{50} of 3.49 µM, suggesting that for cAMP signaling in $SW10_{WT}$ cells, FT_2Fc exhibited higher efficacy but slightly lower potency when compared to previously reported results for FT (Kuffer et al., 2016). Then, we assessed the levels of phosphorylated AKT (pAKT) in SW10 cells upon FT_2Fc treatment (Fig. 2c). $SW10_{WT}$ cells, but not $SW10_{\Delta Adgrg6}$ cells showed a time-dependent increase in AKT phosphorylation when incubated with FT_2Fc. These results suggest that FT_2Fc acted as a ligand of Adgrg6 and activated intracellular pathways similarly to FT.

Establishing a functional read out for in vivo assay

In order to monitor if FT_2Fc is functional in vivo, we injected ZH3 mice intravenously (i.v.) with either FT (600 µg) or FT_2Fc (10 mg/Kg bodyweight). AKT phosphorylation was measured in sciatic nerve lysates by western blotting (Fig. 3a,b). FT injected mice showed a significant increase in the levels of pAKT after 30 minutes (relative pAKT change based on quantitative analysis of western blots: control 1.00 ± 0.05(*3*); FT 1.53 ± 0.11(*3*); $p = 0.0116$; mean ± SEM(*n*); unpaired t-test), whereas FT_2Fc did not elicit an acute increase in AKT phosphorylation (control 1.00 ± 0.04(*4*); FT_2Fc 0.99 ± 0.02(*4*); mean ± SEM(*n*); $p = 0.8560$; unpaired t-test). Additionally, no significant increase in pAKT levels could be detected after 6 days of FT_2Fc treatment (control 1.00 ± 0.07(*3*); FT_2Fc 1.14 ± 0.02*(3);* mean ± SEM(*n*); $p = 0.1356$; unpaired t-test). This result was not unexpected since FT_2Fc is a larger molecule and predicted to diffuse at a slower rate to the target tissue as compared to FT. Accordingly, acute in vivo activity might be difficult to capture with our assay. We therefore proceeded with long-term FT_2Fc treatment of ZH3 mice to assess therapeutic effects upon chronic exposure. As a read-out we aimed at identifying early protein expression changes. The transcription factor Egr2 (Krox20) is required for myelin maintenance (Decker et al., 2006) and has previously been shown to be decreased in ZH3 mice (Kuffer et al., 2016). We collected sciatic nerves from ZH3 mice at various ages and found that Egr2 expression levels progressively decreased starting at 5 months of age

when compared to wild type (WT) C57BL6/J mice (Fig. 3c,d). The protein markers of repair Schwann cells, c-Jun and GFAP, were increased in ZH3 mice already at 1 and 3 months, respectively (Fig. 3c,d). We planned to use these early signs of peripheral nerve damage as a readout to assess the effect of FT_2Fc treatment in a chronic prophylactic treatment study.

In vivo pharmacokinetics of FT_2Fc

To determine a suitable treatment regime for the in vivo experiments, we performed pharmacokinetic studies with FT_2Fc in ZH3 mice. ZH3 mice were injected either i.v. or intraperitoneally (i.p.) with FT_2Fc (5 or 10 mg/Kg). Blood samples were collected at different time points after a single injection (1 h up to 8 days) and FT_2Fc levels were monitored in the serum by western blotting with Fab83. The distribution phase of FT_2Fc was similar after 1 h post injection when comparing i.v. and i.p. injection (Fig. 3e). Thus, we proceeded with i.p. injections for further experiments. In the elimination phase, FT_2Fc followed first order elimination kinetics with an exponential decrease of serum levels over time (Fig. 3f). Based on the serum level – time profile during the elimination phase the terminal serum half-life of FT_2Fc was estimated to be 45 h (Fig. 3g). This duration was deemed sufficiently long for chronic FT_2Fc treatment in mice.

Chronic treatment fails to rescue the myelination in ZH3 mice

We next examined if chronic administration of FT_2Fc in ZH3 mice would rescue the demyelinating neuropathy. We designed a prophylactic study in which treatment was started at 1 month of age, when signs of demyelination are not yet present in ZH3 mice (Bremer et al., 2010; Nuvolone et al., 2016) (Fig. 4a). ZH3 mice were injected i.p. three times per week (based on the 45 h half-life of FT_2Fc) with 8 mg/Kg FT_2Fc or control treatment for a total of 4 months. We additionally included WT mice, which received the same treatment as ZH3 mice. Blood samples were collected at 1 and 2 months after treatment start. Serum levels of FT_2Fc were comparable at both time points (Fig. 4b), indicating that the half-life of FT_2Fc did not decrease over time and that mice did not generate antibodies against FT_2Fc (Chirmule et al., 2012; Zhou et al., 2013). Furthermore, there was no difference in body weight between the treatment

groups (Fig. 4c). At the end of the chronic treatment mice were sacrificed and sciatic nerves were collected for protein analysis (Fig. 4d). GFAP levels were increased whereas Egr2 levels were decreased in sciatic nerves of ZH3 mice when compared to WT mice. However, treatment with FT_2Fc did not rescue the increase of GFAP nor the decrease in Egr2 levels. C-Jun levels were not increased in ZH3 mice when compared to WT mice, nor did FT_2Fc treatment change c-Jun levels. As is expected at the age of 5 months, sciatic nerves of ZH3 mice showed no conspicuous morphological signs of demyelination (Bremer et al., 2010; Nuvolone et al., 2016), and no morphological alterations were induced by FT_2Fc treatment (Fig. 4e,f).

Certain phenotypes in early generations of PrP knockout mice were found to be poorly reproducible and seem to represent genetic confounders (Nuvolone et al., 2016; Wulf et al., 2017). The development of peripheral demyelination, however, was confirmed in ZH3 mice that have a pure C57BL6/J background (Nuvolone et al., 2016). Based on the time course of macrophage infiltrations, the disease seemed to manifest later than described in previous reports on mice with mixed genetic background (Bremer et al., 2010). The early reduction in nerve conduction velocity has not been re-assessed in ZH3 mice. In electrophysiological investigations performed at the end of FT_2Fc treatment, we did not detect a decrease in nerve conduction velocity in ZH3 mice when compared to WT mice (Fig. 5a,b). This suggests that the ZH3 mice used in the experiments reported here had not developed electrophysiological signs of demyelination at the age of 5 months and that these investigations were not a telling readout for a treatment effect in our study. Indeed, we could not detect any differences in nerve conduction velocity or compound muscle action potential amplitude between treatment groups (Fig. 5a-c). No polyphasic compound muscle action potentials were recorded, and electromyography of the foot muscles showed no pathological spontaneous activity.

FT_2Fc treatment elicits gene expression changes which are deleterious in skeletal muscle

In the absence of a rescue of protein markers in ZH3 mice upon chronic FT_2Fc treatment, we postulated that FT_2Fc either did not reach the precise destination in the sciatic nerve or did not activate the desired myelinotrophic signalling pathways. To assess FT_2Fc induced changes in

an unbiased and genome-wide manner, we investigated the transcriptome of sciatic nerves from FT_2Fc treated and control mice by RNA sequencing. Additionally, we sequenced sciatic nerves of untreated WT and ZH3 mice at 4 and 13-15 months.

Unsupervised clustering based on the 100 genes with the highest variance across all samples showed a separation between FT_2Fc treated and control treated ZH3 mice (Fig. 6a). Based on published datasets, we assembled a list of genes that are important for the repair Schwann cell phenotype (Arthur-Farraj et al., 2017). ZH3 mice showed a mild increase of these genes at 4 months and a strong upregulation at 13-15 months (Fig. 6b). We did not observe a change in expression of any of these genes upon FT_2Fc treatment (Fig. 6b), which is in line with the absence of changes in repair Schwann cell markers at the protein level. Instead, functional gene ontology analysis revealed that FT_2Fc specifically induced a downregulation of genes associated with muscle contraction and organization of actin filaments and sarcomeres (Table 1, Fig. 6c). Our sciatic nerve bulk RNA sequencing analysis did not allow us to infer in which cell type these genes were differentially expressed. We therefore explored previously published single cell RNA sequencing data from healthy and injured sciatic nerves (Carr et al., 2019). Several genes that were differentially expressed upon FT_2Fc treatment are enriched in perivascular cells and vascular smooth muscle cells (Des, Sh3bgr, Tpm1, Ldb3) or belong to mesenchymal cell clusters (Tnnt3, Cmya5, Pygm, Eno3). In contrast, genes that are expressed specifically in Schwann cells did not change their expression profile upon FT_2Fc treatment.

These unexpected experimental observations led us to consider previous studies that showed a necrotizing myopathy in mice overexpressing PrP (Westaway et al., 1994; Huang et al., 2007). We wondered whether treatment with FT_2Fc may have mimicked PrP overexpression and induced gene expression changes similar to those involved in the myopathy phenotype rather than acting as a ligand to Adgrg6. We therefore compared the transcriptomic changes in FT_2Fc treated sciatic nerves to gene expression changes in the tibialis anterior muscle upon inducible PrP overexpression (Fig. 7a,b). While the overall correlation between the datasets was low, a noteworthy overlap was observed among the downregulated genes. Specifically,

35% of genes that were significantly downregulated (FDR < 0.05) by FT_2Fc were also downregulated in PrP overexpressing muscle. This suggests that FT_2Fc treatment might have triggered pathways similar to those caused by PrP overexpression. However, the muscle tissue of FT_2Fc-treated mice did not show any myopathic changes (Fig. 7c).

In conclusion, the transcriptomic analysis showed that chronically administered FT_2Fc had reached the sciatic nerve and elicited a specific pharmacodynamic effect. Yet the detected gene expression changes did not indicate an activation of Adgrg6-mediated myelination signalling. Instead, the downregulation of cytoskeleton proteins and contractile elements was reminiscent of the toxic effects of PrP overexpression.

Discussion

The treatment options for many peripheral nerve diseases are limited, and despite the remarkable ability for repair in the PNS, regeneration in intrinsic peripheral neuropathies or after nerve injury is often incomplete. Schwann cells are crucial for the function and maintenance of peripheral nerves and may represent interesting targets to boost the endogenous repair capacity of the PNS.

Many approved drugs target G-protein coupled receptors, and therefore Adgrg6 may represent an attractive potential target to stimulate repair in peripheral neuropathies or after nerve damage. We here exploited a natural Adgrg6 agonist, PrP, to design a molecule targeting Adgrg6 for the treatment of peripheral nerve disease. The fusion of PrP's myelinotrophic domain to an Fc-fragment (FT_2Fc) yielded a molecule with sufficiently long half-life, making it feasible for in vivo treatment. Several Fc-fusion based drugs (also termed immunoadhesins) have been approved for therapeutic use in humans (Strohl, 2015). Importantly, immunoadhesins are intrinsically dimeric. In the case of sufficiently dense targets, this allows for two-point binding. The theoretical avidity of such binding corresponds to the product of the monomeric binding affinity and can be extremely high (Czajkowsky et al., 2012; Liu et al., 2014).

We attempted a proof-of-principle study by prophylactically administering FT_2Fc to ZH3 mice, which develop a slowly progressive peripheral demyelinating neuropathy during their lifetime (Bremer et al., 2010). However, FT_2Fc did not activate the desired pro-myelination signaling pathways in our treatment study and we failed to detect a therapeutic effect in vivo. Instead, we detected a downregulation of cytoskeleton-related genes, reminiscent of the changes seen in skeletal muscle of PrP overexpressing mice developing a necrotizing myopathy (Huang et al., 2007). While comparison of the transcriptional changes in different tissues must be interpreted with caution, the possibility of myotoxicity induced by a PrP-based agent should not be discounted.

Myelination and the maintenance of myelin are controlled by tightly balanced reciprocal signalling between Schwann cells, axons and extracellular matrix (Salzer, 2015). Inappropriate or excessive activation of involved signalling pathways can have detrimental effects on myelin development, maintenance or repair (Figlia et al., 2017; Cervellini et al., 2018). In our chronic treatment study, FT_2Fc did not negatively affect myelin maintenance as assessed by biochemical, morphological and electrophysiological investigations.

Limitations of this study

Several reasons may explain the lack of a demonstrable treatment effect of FT_2Fc in vivo. Peripheral nerve damage in ZH3 mice at the age investigated here was only mild, as indicated by the lack of electrophysiological signs of demyelination. But even at the protein level, no amelioration of disease markers was achieved by chronic FT_2Fc treatment. We wondered whether this may have been caused by disadvantageous pharmacokinetic properties of FT_2Fc. As a relatively large molecule, FT_2Fc might not have reached Adgrg6 on Schwann cells in sufficient quantities. However immunoglobulins, which are three times larger than FT_2Fc, were reported to cross the blood-nerve-barrier (Seitz et al., 1985). Alternatively, an uneven distribution caused for example by binding of FT_2Fc to Fcγ-receptors in various tissues could have sequestered FT_2Fc from the peripheral nerves. Reassuringly, the transcriptomic analysis revealed specific gene expression changes in the sciatic nerves of FT_2Fc treated mice,

488 suggesting that FT_2Fc reached its destination and was pharmacodynamically active. Yet FT_2Fc
489 did not activate the desired signaling pathways. The dimeric nature of FT_2Fc could alter its
490 biological activity when compared to monomeric FT and endogenous PrP. A soluble dimeric
491 full-length PrP was previously shown to have different properties that endogenous PrP with
492 regard to its pathologic structural conversion (Meier et al., 2003). Whether the dimeric full-
493 length PrP is able to sustain its physiological function in myelin homeostasis has not been
494 investigated by Meier *et al*. Moreover, oligomerization of receptors including adhesion G-
495 protein coupled receptors, contributes to biased signaling (Ferre et al., 2014; Franco et al.,
496 2016). A dimeric ligand such as FT_2Fc may exhibit novel binding properties, induce receptor
497 homo- or hetero-oligomerization and activate different intracellular signaling pathways in vivo.
498 Our in vitro studies with FT_2Fc showed increased cAMP elevation and prolonged AKT
499 phosphorylation when compared to FT. While we interpreted these results as evidence for a
500 high potency and stability of FT_2Fc, they could also indicate biased agonism and contribute to
501 the unexpected pharmacodynamics properties of FT_2Fc in vivo (Pupo et al., 2016).

502 *Conclusions*

503 To the best of our knowledge, this study represents the first attempt to target Adgrg6 activation
504 for treating peripheral nerve demyelination in vivo. Although our treatment regimen was not
505 successful, Adgrg6 should not be discarded as a possible therapeutic target for peripheral
506 nerve diseases. For example, FT_2Fc could be tested in more rapidly progressive models of
507 peripheral demyelination such as autoimmune peripheral neuropathies (Salomon et al., 2001).
508 Moreover, the pharmacokinetics and pharmacodynamics of Adgrg6 ligands might be optimized
509 by modifications such as coupling FT to polyethylene glycol or dendrimers or by designing a
510 bispecific molecule targeting Adgrg6 and thereby directing FT to its receptor. Such strategies
511 may be hampered by the blood-nerve barrier, which may hinder access of the therapeutic
512 compound to Adgrg6 on Schwann cells. Encouragingly, two studies have identified novel
513 agonists of Adgrg6 by drug screening in zebrafish (Bradley et al., 2019; Diamantopoulou et al.,
514 2019). Such small-molecule drugs may exhibit better penetration into nerves than the

515 biological macromolecule studied here and could be leveraged to target Adgrg6 in vivo. Future
516 studies should explore these alternative therapeutic strategies utilizing a variety of disease
517 models.

518

519 **Acknowledgements:** AH is the recipient of an MD PhD fellowship from Swiss National
520 Foundation (project number 323530_171140). AA is the recipient of an Advanced Grant of the
521 European Research Council, the Nomis Foundation and SystemsX.ch. AS and AKKL are
522 recipients of grants from the Synapsis Foundation. KVT is the recipient of a senior
523 professorship research grant by the University of Würzburg. AA and GS are the recipients of
524 the Swiss National Foundation Sinergia grant CRSII5 183563.

525 We thank the following people for their contributions: Mirzet Delic, Ezio Luongo and Olga
526 Romashkina for technical help with mouse experiments; Rita Moos and Simone Hornemann
527 for advice and technical help regarding protein purification; FGCZ staff (specifically Maria
528 Domenica Moccia and Giancarlo Russo) for generation of RNA sequencing data and
529 bioinformatic support; Jorge A.A. Pereira and Elisabeth J. Rushing for helpful advice,
530 Alexander Henzi for support with R programming and statistical analyses.

531 **Conflict of interest statement:** The authors declare no competing financial interests.

532 **Author's contributions:** AA, AH, AS and AKKL designed experiments, analysed data and
533 wrote the manuscript. AH and AS performed design, expression and characterization of FT_2Fc.
534 JM and AH designed and performed the thermal shift assay, JM provided advise for protein
535 purification. AKKL and AH performed the cAMP assays and injection of mice with FT-peptide.
536 AH performed all mouse experiments with FT_2Fc and analyses thereof, including RNA
537 sequencing data analysis. CS contributed to RNA sequencing data analysis and manuscript
538 writing. RR and SS performed experiments with PrP overexpressing mice. KVT and AH
539 performed electrophysiological analyses. All authors approved the final version.

References

Arthur-Farraj PJ, Morgan CC, Adamowicz M, Gomez-Sanchez JA, Fazal SV, Beucher A, Razzaghi B, Mirsky R, Jessen KR, Aitman TJ (2017) Changes in the Coding and Non-coding Transcriptome and DNA Methylome that Define the Schwann Cell Repair Phenotype after Nerve Injury. Cell Rep 20:2719-2734.

Baiardi S, Redaelli V, Ripellino P, Rossi M, Franceschini A, Moggio M, Sola P, Ladogana A, Fociani P, Magherini A, Capellari S, Giese A, Caughey B, Caroppo P, Parchi P (2019) Prion-related peripheral neuropathy in sporadic Creutzfeldt-Jakob disease. J Neurol Neurosurg Psychiatry 90:424-427.

Boerboom A, Dion V, Chariot A, Franzen R (2017) Molecular Mechanisms Involved in Schwann Cell Plasticity. Front Mol Neurosci 10:38.

Bradley EC, Cunningham RL, Wilde C, Morgan RK, Klug EA, Letcher SM, Schoneberg T, Monk KR, Liebscher I, Petersen SC (2019) In vivo identification of small molecules mediating Gpr126/Adgrg6 signaling during Schwann cell development. Ann N Y Acad Sci 1456:44-63.

Bremer J, Baumann F, Tiberi C, Wessig C, Fischer H, Schwarz P, Steele AD, Toyka KV, Nave KA, Weis J, Aguzzi A (2010) Axonal prion protein is required for peripheral myelin maintenance. Nat Neurosci 13:310-318.

Carr MJ, Toma JS, Johnston APW, Steadman PE, Yuzwa SA, Mahmud N, Frankland PW, Kaplan DR, Miller FD (2019) Mesenchymal Precursor Cells in Adult Nerves Contribute to Mammalian Tissue Repair and Regeneration. Cell Stem Cell 24:240-256 e249.

Cervellini I, Galino J, Zhu N, Allen S, Birchmeier C, Bennett DL (2018) Sustained MAPK/ERK Activation in Adult Schwann Cells Impairs Nerve Repair. J Neurosci 38:679-690.

Chirmule N, Jawa V, Meibohm B (2012) Immunogenicity to therapeutic proteins: impact on PK/PD and efficacy. AAPS J 14:296-302.

Collins AM (2016) IgG subclass co-expression brings harmony to the quartet model of murine IgG function. Immunol Cell Biol 94:949-954.

567 Craik DJ, Fairlie DP, Liras S, Price D (2013) The future of peptide-based drugs. Chem Biol
568 Drug Des 81:136-147.
569 Czajkowsky DM, Hu J, Shao Z, Pleass RJ (2012) Fc-fusion proteins: new developments and
570 future perspectives. EMBO Mol Med 4:1015-1028.
571 Dashivets T, Thomann M, Rueger P, Knaupp A, Buchner J, Schlothauer T (2015) Multi-Angle
572 Effector Function Analysis of Human Monoclonal IgG Glycovariants. PLoS One
573 10:e0143520.
574 Decker L, Desmarquet-Trin-Dinh C, Taillebourg E, Ghislain J, Vallat JM, Charnay P (2006)
575 Peripheral myelin maintenance is a dynamic process requiring constant Krox20
576 expression. J Neurosci 26:9771-9779.
577 Diamantopoulou E, Baxendale S, de la Vega de Leon A, Asad A, Holdsworth CJ, Abbas L,
578 Gillet VJ, Wiggin GR, Whitfield TT (2019) Identification of compounds that rescue otic
579 and myelination defects in the zebrafish adgrg6 (gpr126) mutant. Elife 8.
580 Dobin A, Davis CA, Schlesinger F, Drenkow J, Zaleski C, Jha S, Batut P, Chaisson M,
581 Gingeras TR (2013) STAR: ultrafast universal RNA-seq aligner. Bioinformatics 29:15-
582 21.
583 Ferre S, Casado V, Devi LA, Filizola M, Jockers R, Lohse MJ, Milligan G, Pin JP, Guitart X
584 (2014) G protein-coupled receptor oligomerization revisited: functional and
585 pharmacological perspectives. Pharmacol Rev 66:413-434.
586 Figlia G, Norrmen C, Pereira JA, Gerber D, Suter U (2017) Dual function of the PI3K-Akt-
587 mTORC1 axis in myelination of the peripheral nervous system. Elife 6.
588 Franco R, Martinez-Pinilla E, Lanciego JL, Navarro G (2016) Basic Pharmacological and
589 Structural Evidence for Class A G-Protein-Coupled Receptor Heteromerization. Front
590 Pharmacol 7:76.
591 Gerber D, Ghidinelli M, Tinelli E, Somandin C, Gerber J, Pereira JA, Ommer A, Figlia G, Miehe
592 M, Nageli LG, Suter V, Tadini V, Sidiropoulos PN, Wessig C, Toyka KV, Suter U (2019)
593 Schwann cells, but not Oligodendrocytes, Depend Strictly on Dynamin 2 Function. Elife
594 8.

595 Hatakeyama M, Opitz L, Russo G, Qi W, Schlapbach R, Rehrauer H (2016) SUSHI: an
596 exquisite recipe for fully documented, reproducible and reusable NGS data analysis.
597 BMC Bioinformatics 17:228.
598 Huang S, Liang J, Zheng M, Li X, Wang M, Wang P, Vanegas D, Wu D, Chakraborty B, Hays
599 AP, Chen K, Chen SG, Booth S, Cohen M, Gambetti P, Kong Q (2007) Inducible
600 overexpression of wild-type prion protein in the muscles leads to a primary myopathy
601 in transgenic mice. Proc Natl Acad Sci U S A 104:6800-6805.
602 Jablonka-Shariff A, Lu CY, Campbell K, Monk KR, Snyder-Warwick AK (2020) Gpr126/Adgrg6
603 contributes to the terminal Schwann cell response at the neuromuscular junction
604 following peripheral nerve injury. Glia 68:1182-1200.
605 Jessen KR, Mirsky R, Morgan L (1991) Role of cyclic AMP and proliferation controls in
606 Schwann cell differentiation. Ann N Y Acad Sci 633:78-89.
607 Koop O, Timmerman V, de Jonghe P, Ringelstein B, Young P, Kuhlenbaumer G (2005)
608 Absence of mutations in the prion-protein gene in a large cohort of HMSN patients.
609 Neuromuscul Disord 15:549-551.
610 Kuffer A, Lakkaraju AK, Mogha A, Petersen SC, Airich K, Doucerain C, Marpakwar R, Bakirci
611 P, Senatore A, Monnard A, Schiavi C, Nuvolone M, Grosshans B, Hornemann S,
612 Bassilana F, Monk KR, Aguzzi A (2016) The prion protein is an agonistic ligand of the
613 G protein-coupled receptor Adgrg6. Nature 536:464-468.
614 Liao Y, Smyth GK, Shi W (2014) featureCounts: an efficient general purpose program for
615 assigning sequence reads to genomic features. Bioinformatics 30:923-930.
616 Liu CJ, Jones DS, 2nd, Tsai PC, Venkataramana A, Cochran JR (2014) An engineered dimeric
617 fragment of hepatocyte growth factor is a potent c-MET agonist. FEBS Lett 588:4831-
618 4837.
619 Meier P, Genoud N, Prinz M, Maissen M, Rulicke T, Zurbriggen A, Raeber AJ, Aguzzi A (2003)
620 Soluble dimeric prion protein binds PrP(Sc) in vivo and antagonizes prion disease. Cell
621 113:49-60.

622 Mogha A, Benesh AE, Patra C, Engel FB, Schoneberg T, Liebscher I, Monk KR (2013) Gpr126
623 functions in Schwann cells to control differentiation and myelination via G-protein
624 activation. J Neurosci 33:17976-17985.
625 Mogha A, Harty BL, Carlin D, Joseph J, Sanchez NE, Suter U, Piao X, Cavalli V, Monk KR
626 (2016) Gpr126/Adgrg6 Has Schwann Cell Autonomous and Nonautonomous
627 Functions in Peripheral Nerve Injury and Repair. J Neurosci 36:12351-12367.
628 Monje PV, Bartlett Bunge M, Wood PM (2006) Cyclic AMP synergistically enhances
629 neuregulin-dependent ERK and Akt activation and cell cycle progression in Schwann
630 cells. Glia 53:649-659.
631 Monje PV, Soto J, Bacallao K, Wood PM (2010) Schwann cell dedifferentiation is independent
632 of mitogenic signaling and uncoupled to proliferation: role of cAMP and JNK in the
633 maintenance of the differentiated state. J Biol Chem 285:31024-31036.
634 Monk KR, Oshima K, Jors S, Heller S, Talbot WS (2011) Gpr126 is essential for peripheral
635 nerve development and myelination in mammals. Development 138:2673-2680.
636 Monk KR, Naylor SG, Glenn TD, Mercurio S, Perlin JR, Dominguez C, Moens CB, Talbot WS
637 (2009) A G protein-coupled receptor is essential for Schwann cells to initiate
638 myelination. Science 325:1402-1405.
639 Neufeld MY, Josiphov J, Korczyn AD (1992) Demyelinating peripheral neuropathy in
640 Creutzfeldt-Jakob disease. Muscle Nerve 15:1234-1239.
641 Nishida N, Tremblay P, Sugimoto T, Shigematsu K, Shirabe S, Petromilli C, Erpel SP, Nakaoke
642 R, Atarashi R, Houtani T, Torchia M, Sakaguchi S, DeArmond SJ, Prusiner SB,
643 Katamine S (1999) A mouse prion protein transgene rescues mice deficient for the
644 prion protein gene from purkinje cell degeneration and demyelination. Lab Invest
645 79:689-697.
646 Nuvolone M, Hermann M, Sorce S, Russo G, Tiberi C, Schwarz P, Minikel E, Sanoudou D,
647 Pelczar P, Aguzzi A (2016) Strictly co-isogenic C57BL/6J-Prnp-/- mice: A rigorous
648 resource for prion science. J Exp Med 213:313-327.

649 Piazza M, Prior TW, Khalsa PS, Appleby B (2020) A case report of genetic prion disease with
650 two different PRNP variants. Mol Genet Genomic Med 8:e1134.
651 Pupo AS, Duarte DA, Lima V, Teixeira LB, Parreiras ESLT, Costa-Neto CM (2016) Recent
652 updates on GPCR biased agonism. Pharmacol Res 112:49-57.
653 Robinson MD, McCarthy DJ, Smyth GK (2010) edgeR: a Bioconductor package for differential
654 expression analysis of digital gene expression data. Bioinformatics 26:139-140.
655 Salomon B, Rhee L, Bour-Jordan H, Hsin H, Montag A, Soliven B, Arcella J, Girvin AM, Padilla
656 J, Miller SD, Bluestone JA (2001) Development of spontaneous autoimmune peripheral
657 polyneuropathy in B7-2-deficient NOD mice. J Exp Med 194:677-684.
658 Salzer JL (2015) Schwann cell myelination. Cold Spring Harb Perspect Biol 7:a020529.
659 Seitz RJ, Heininger K, Schwendemann G, Toyka KV, Wechsler W (1985) The mouse blood-
660 brain barrier and blood-nerve barrier for IgG: a tracer study by use of the avidin-biotin
661 system. Acta Neuropathol 68:15-21.
662 Senatore A, Frontzek K, Emmenegger M, Chincisan A, Losa M, Reimann R, Horny G, Guo J,
663 Fels S, Sorce S, Zhu C, George N, Ewert S, Pietzonka T, Hornemann S, Aguzzi A
664 (2020) Protective anti-prion antibodies in human immunoglobulin repertoires.
665 bioRxiv:2020.2002.2005.933721.
666 Skedsmo FS, Malachin G, Vage DI, Hammervold MM, Salvesen O, Ersdal C, Ranheim B,
667 Stafsnes MH, Bartosova Z, Bruheim P, Jaderlund KH, Matiasek K, Espenes A, Tranulis
668 MA (2020) Demyelinating polyneuropathy in goats lacking prion protein. FASEB J
669 34:2359-2375.
670 Sorce S, Nuvolone M, Russo G, Chincisan A, Heinzer D, Avar M, Pfammatter M, Schwarz P,
671 Delic M, Hornemann S, Sanoudou D, Scheckel C, Aguzzi A (2020) Genome-wide
672 transcriptomics identifies an early preclinical signature of prion infection.
673 bioRxiv:2020.2001.2010.901637.
674 Strohl WR (2015) Fusion Proteins for Half-Life Extension of Biologics as a Strategy to Make
675 Biobetters. BioDrugs 29:215-239.

676 Westaway D, DeArmond SJ, Cayetano-Canlas J, Groth D, Foster D, Yang SL, Torchia M,
677 Carlson GA, Prusiner SB (1994) Degeneration of skeletal muscle, peripheral nerves,
678 and the central nervous system in transgenic mice overexpressing wild-type prion
679 proteins. Cell 76:117-129.
680 Wozniak-Knopp G, Stadlmann J, Ruker F (2012) Stabilisation of the Fc fragment of human
681 IgG1 by engineered intradomain disulfide bonds. PLoS One 7:e30083.
682 Wulf MA, Senatore A, Aguzzi A (2017) The biological function of the cellular prion protein: an
683 update. BMC Biol 15:34.
684 Xu E, Shao W, Jiang H, Lin T, Gao R, Zhou X (2019) A Genetic Variant in GPR126 Causing a
685 Decreased Inclusion of Exon 6 Is Associated with Cartilage Development in Adolescent
686 Idiopathic Scoliosis Population. Biomed Res Int 2019:4678969.
687 Zhou L, Hoofring SA, Wu Y, Vu T, Ma P, Swanson SJ, Chirmule N, Starcevic M (2013)
688 Stratification of antibody-positive subjects by antibody level reveals an impact of
689 immunogenicity on pharmacokinetics. AAPS J 15:30-40.
690 Zielasek J, Martini R, Toyka KV (1996) Functional abnormalities in P0-deficient mice resemble
691 human hereditary neuropathies linked to P0 gene mutations. Muscle Nerve 19:946-
692 952.

693

694

Figure legends

Figure 1: Characterization of FT_2Fc.

a) Design of FT_2Fc. FT was fused to mIgG1-Fc at the hinge, thereby replacing the antigen-binding fragment (Fab) and forming a homodimeric Fc-fusion protein. **b)** FT_2Fc was secreted by 293-F cells after transient transfection and was present in the cell culture supernatant as a homodimer with a size of 56 kD. Under reducing conditions (+DTT), FT_2Fc was present as a monomer. FT_2Fc was detected in western blotting by antibodies targeting the Fc-fragment and a Fab specific for FT (Fab83). Supernatant from non-transfected cells (NT) was used as negative control. **c)** Sandwich ELISA of serially diluted cell culture supernatant from cells transfected with FT_2Fc showed a sigmoidal curve. The optical-density (OD) - dilution curves were fitted using the four-parameter logistic nonlinear regression model (dashed lines, R^2 = 0.94 for FT_2Fc). Only background signal was detected in supernatant from cells transfected with the empty vector control (EVC) or non-transfected cells (NT), or when the plate was coated with BSA instead of Fab83. **d)** Design of the immunoprecipitation assay (left). Western blots of eluates and beads boiled in sample loading buffer (right). FT_2Fc was captured in cell culture supernatant by beads coated with Fab83 and was eluted with a peptide specifically competing for the Fab83 binding site, but not with a non-competing peptide. The western blot from the beads confirmed that FT_2Fc (size of specific bands marked with *) was bound to the beads in all conditions. **e)** In the thermal shift assay, the unfolding of FT_2Fc with increasing temperature was monitored using a fluorescent dye. The curve was fitted to the Boltzmann equation (dashed line, R^2 = 0.99). The inflection point at 74.5 °C corresponds to the melting temperature of FT_2Fc in 20 mM sodium phosphate, pH 7.

Figure 2: Activation of Adgrg6 by FT_2Fc in vitro.

a) FT and FT_2Fc elicited an increase in cAMP levels in $SW10_{WT}$ cells, but not in $SW10_{\Delta Adgrg6}$ cells. cAMP levels were measured 20 min after treatment with 5 µM FT or 2.5 µM FT_2Fc. To account for variability in cAMP levels across cell lines, cAMP was expressed as x-fold change to the average of the controls (PBS and 20 mM sodium phosphate buffer) for each of the 4

722 independent experiments. One-way ANOVA for selected comparisons, Sidak's multiple
723 comparisons test: in $SW10_{WT}$ FT vs. PBS $p = 0.0392$, FT_2Fc vs. buffer $p = 0.0035$. In
724 $SW10_{\Delta Adgrg6}$ FT and FT_2Fc vs. controls $p > 0.05$. **b)** $SW10_{WT}$ cells were incubated with
725 increasing concentrations of FT_2Fc. cAMP levels increased up to a maximum of a 9-fold
726 change when compared to untreated cells. Nonlinear regression analysis revealed an EC_{50} of
727 3.49 µM. For the curve fitting with the four-parameter logistic regression model (dashed line,
728 $R^2 = 0.78$) only values from 0-8 µM (2-3 replicates per concentration) were used, because the
729 strongly reduced activity at 9 and 10 µM would have confounded the analysis. **c)** $SW10_{WT}$, but
730 not $SW10_{\Delta Adgrg6}$ cells showed a time-dependent increase in AKT phosphorylation upon
731 treatment with 1 µM FT_2Fc. Quantification of 5 independent experiments (left), representative
732 western blot of cell lysates (right). Comparison of $SW10_{WT}$ to $SW10_{\Delta Adgrg6}$ cells with two-way
733 ANOVA followed by Sidak's multiple comparisons test: at 10 min, 15 min and 30 min $p <$
734 0.0001, at 5 min and 10 min $p > 0.05$. ns = not significant.

735 *Figure 3: Establishment of readout and pharmacokinetics.*

736 **a)** AKT phosphorylation increased in sciatic nerves of ZH3 mice 30 min after injection of 600
737 µg FT. As control (ctrl), mice were injected with an inactive peptide, in which lysine residues
738 have been replaced with alanine residues (Kuffer et al., 2016). In mice injected with FT_2Fc (10
739 mg/Kg), no significant change in AKT phosphorylation was detected after 30 min when
740 compared to mIgG injected mice. Square brackets in western blots indicate left and right sciatic
741 nerves taken from one mouse. The average value was used for quantification. **b)** AKT
742 phosphorylation did not increase after six consecutive FT_2Fc injections. **c,d)** ZH3 mice
743 exhibited an age-dependent decrease in sciatic nerve Egr2 levels and a concomitant increase
744 in GFAP and c-Jun levels. Western blots of sciatic nerve lysates are shown in **(c)**, result of
745 densitometry in **(d)**. **e)** ZH3 mice were i.v. ($n = 2$) or i.p. ($n = 2$) injected with FT_2Fc (5 mg/Kg)
746 and FT_2Fc serum levels were monitored by western blotting with Fab83 at 1, 6 and 24 h after
747 injection. A serum sample from a mouse injected with mIgG (5 mg/Kg) was used as negative
748 control. The early serum level – time course was similar in i.v. and i.p. injected mice. **f)** ZH3
749 mice were i.p. injected with 10 mg/Kg FT_2Fc and blood samples were collected from 1 to 8

750 days post injection. The elimination of FT_2Fc from serum followed first order elimination
751 kinetics. **g)** Serum level values (normalized to the level at 23 h post injection) were plotted on
752 a semi-logarithmic graph and fitted with nonlinear least-squares analysis (dashed line, R^2 =
753 0.92) to calculate the terminal serum half-life of FT_2Fc. The serum half-life was estimated to
754 be 45 h with a 95% confidence interval of 37-58 h. The number of mice investigated per time
755 point (*n*) is indicated above the points.

756 *Figure 4: Chronic administration of FT_2Fc.*

757 **a)** Design of the prophylactic treatment experiment in ZH3 and WT mice. Starting at 1 month
758 of age, ZH3 and WT mice were injected with FT_2Fc (or control treatment) 3 times per week
759 until the age of 5 months. Bars with grey shades show expected changes in protein levels with
760 dark and light grey meaning high and low levels, respectively. **b)** FT_2Fc serum levels were
761 measured 2 days after the last injection. Representative western blot showing serum levels for
762 4 ZH3 mice after 1 and 2 months of treatment. FT_2Fc serum levels did not decrease after 2
763 months of treatment when compared to the level at 1 month (n = 8, paired t-test, p = 0.3529),
764 suggesting that FT_2Fc half-life was unaltered. **c)** Bodyweight was not significantly different
765 between treatment groups (as analysed by two-way repeated measures ANOVA, $p > 0.05$).
766 Body weight was recorded at every injection time point for all the mice in the chronic treatment
767 study and is here shown for week 1 to 6 of treatment as percentage of the body weight at
768 treatment start (reference). **d)** Representative western blots and quantification for levels of
769 GFAP, c-Jun and Egr2 in sciatic nerves. GFAP levels were significantly higher in ZH3 mice
770 compared to WT mice, but no significant change was induced by FT_2Fc compared to buffer
771 treatment (one-way ANOVA for selected comparisons, Bonferroni's multiple comparisons test:
772 ZH3 vs. WT for buffer treated mice p = 0.0345, for FT_2Fc treated mice p = 0.0343. FT_2Fc vs.
773 buffer treated mice, both ZH3 and WT $p > 0.05$). C-Jun levels were not decreased in ZH3
774 compared to WT mice, and no significant change in c-Jun levels was induced by FT_2Fc
775 treatment (one-way ANOVA for selected comparisons, Bonferroni's multiple comparisons test,
776 $p > 0.05$). Egr2 levels were significantly lower in ZH3 mice compared to WT mice, but FT_2Fc
777 treatment did not induce a significant change in any genotype (one-way ANOVA for selected

778 comparisons, Bonferroni's multiple comparisons test: ZH3 vs. WT for buffer treated mice $p <$
779 0.0001, for FT_2Fc treated mice $p = 0.0044$. FT_2Fc vs. buffer treated mice, both ZH3 and WT p
780 > 0.05). Protein levels were expressed as fold change the average level in buffer treated ZH3
781 mice. **e)** Toluidine-blue stained semithin sections of sciatic nerves. No difference in fibre
782 morphology was detected between treatment groups in our ZH3 mouse specimens. Scale bar
783 50 µM. **f)** Number of myelinated axons per mm^2 in sciatic nerves of ZH3 mice revealed no
784 difference between treatment groups (comparison of FT_2Fc and IgG treated to buffer treated
785 mice by one-way ANOVA followed by Dunnett's multiple comparisons test, $p > 0.05$). ns = not
786 significant.

787 *Figure 5: Electrophysiological studies.*

788 All tests and calculations were done with the examiners masked as to treatment and strain
789 allocation. **a)** Motor nerve conduction velocities (NCV) for WT and ZH3 mice. There was no
790 significant difference between WT and ZH3 mice, or between FT_2Fc treated and buffer treated
791 mice (one-way ANOVA for indicated comparisons, Bonferroni's multiple comparisons test, $p >$
792 0.05). **b)** Compound sensory NCV (csNCV) for WT and ZH3 mice. Again, there was no
793 significant difference between WT and ZH3 mice, or FT_2Fc treated and buffer treated mice
794 (one-way ANOVA for indicated comparisons, Bonferroni's multiple comparisons test, $p > 0.05$).
795 **c)** The ratio of proximal to distal compound muscle action potential (CMAP) amplitude was not
796 significantly different when comparing ZH3 to WT mice or FT_2Fc to buffer treated mice (one-
797 way ANOVA for indicated comparisons, Bonferroni's multiple comparisons test, $p > 0.05$). ns
798 = not significant.

799 *Figure 6: RNA sequencing of sciatic nerves from FT_2Fc treated mice.*

800 **a)** Hierarchical clustering analysis based on the 100 genes with the highest variance across
801 all samples showed a separation between FT_2Fc treated mice and control mice ($n = 4$ per
802 treatment). **b)** Heatmap of the selected repair Schwann cell genes. The red-blue colour key is
803 based on the row-wise Z-scores. 4 months old ZH3 mice ($n = 3$) showed a mild, 13-15 months
804 old ZH3 mice ($n = 4$) a pronounced upregulation of these genes when compared to age-

matched WT mice. No difference was detected in FT_2Fc treated ZH3 mice (*n* = 4) compared to buffer treated mice (*n* = 4). **c)** Volcano plot showing differentially expressed genes in sciatic nerves of FT_2Fc treated compared to buffer treated mice. Genes with FDR < 0.05 were considered significantly up- or downregulated (43 downregulated genes, 1 upregulated gene). Genes involved in actin binding are labelled in the plot. Log2FC = log2 fold change.

Figure 7: Genes downregulated by FT_2Fc show similar changes in PrP-overexpressing muscle.

a) Log2 fold change (log2FC) for significantly downregulated genes (*n* = 43, based FDR < 0.05) in sciatic nerves of FT_2Fc treated compared to buffer treated mice and corresponding log2FC in tibialis anterior muscle of PrP overexpressing mice. * marks genes which were also significantly downregulated in muscle based on FDR < 0.05 (*n* = 15). Grouping of genes according to common functions was based on a manual search in the UniProt database. **b)** Scatterplot comparing gene expression changes in muscle of PrP overexpressing mice and sciatic nerves of FT_2Fc treated mice. 1229 and 43 genes were significantly (FDR < 0.05) downregulated in muscle and nerve, respectively, with 15 of these genes overlapping. Grey line represents linear regression. Pearson's correlation coefficient r = 0.09. **c)** 10 µM Gomori trichrome stained frozen sections of gastrocnemius muscle from FT_2Fc and buffer treated ZH3 mice. Muscle fibre morphology was similar in buffer and FT_2Fc treated mice. No myopathic changes were detected in FT_2Fc treated mice. Scale bar 20 µM.

Table 1) Gene ontology analysis of differentially expressed genes in sciatic nerves of FT_2Fc treated compared to buffer treated mice. The complete list of overrepresented categories is shown in Supplementary Table S1.

Supplementary Material

Figures S1-S4: Original western blot images and coomassie gels from all figures.

The uncropped images have been inverted and autoscaled using the Quantify One software (Biorad). Lanes with protein size markers (Protein Precision Plus, Biorad) are indicated with M. Relevant size markers are marked with the respective size in kD. The specific band is

marked with * when additional non-specific bands are present. Irrelevant lanes that have been excluded from the main figures are marked with x. The samples that were loaded in these lines are described in annotations. Lanes that were left empty are marked with e.

Table S1: Complete list of overrepresented GO categories in sciatic nerves of FT_2Fc treated compared to buffer treated mice.

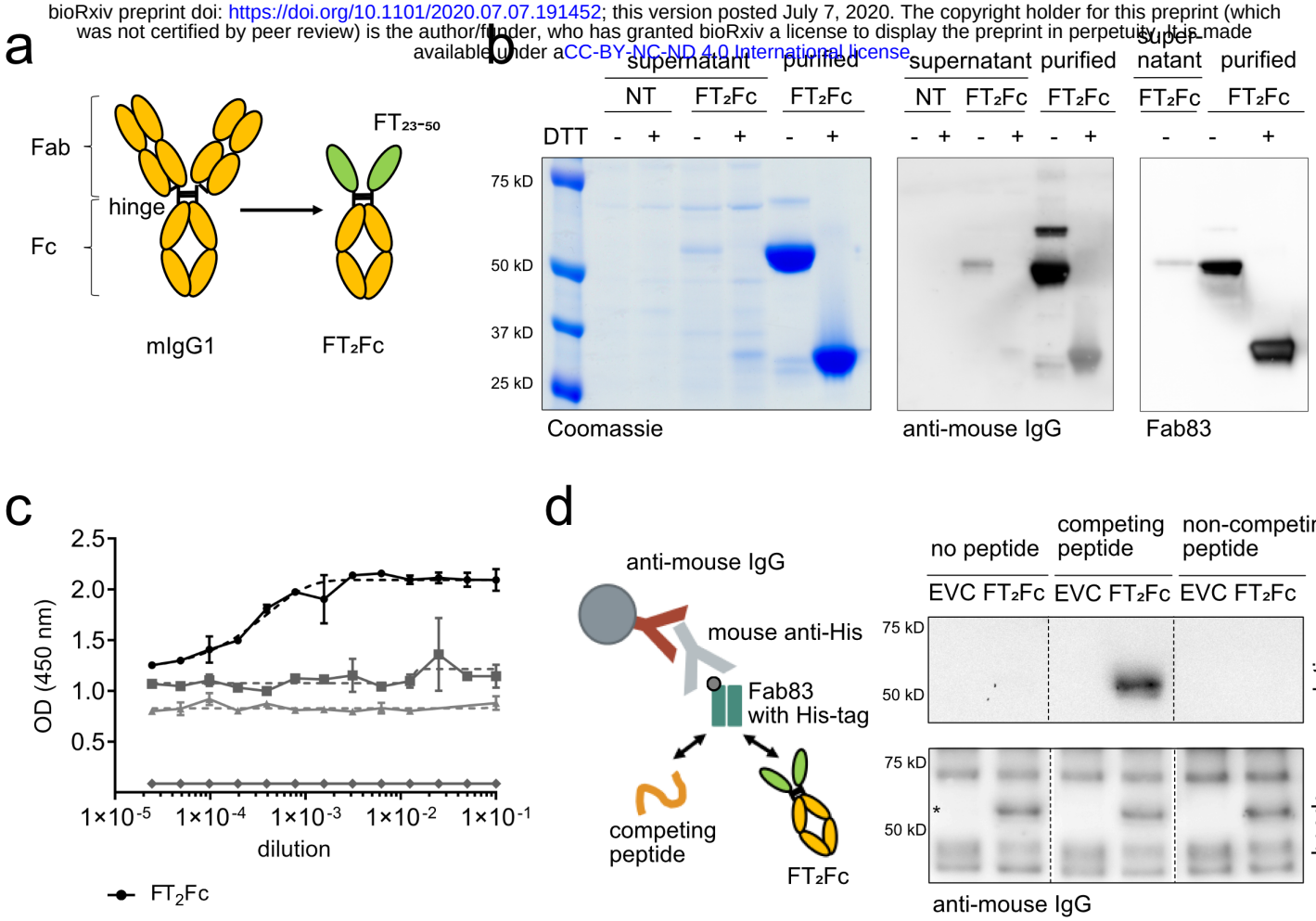

a

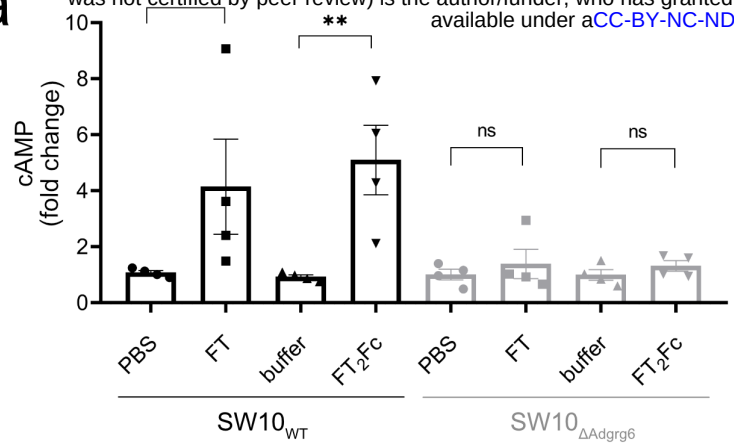

b

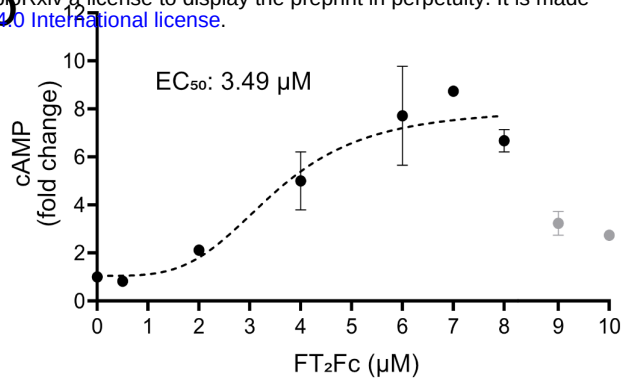

c

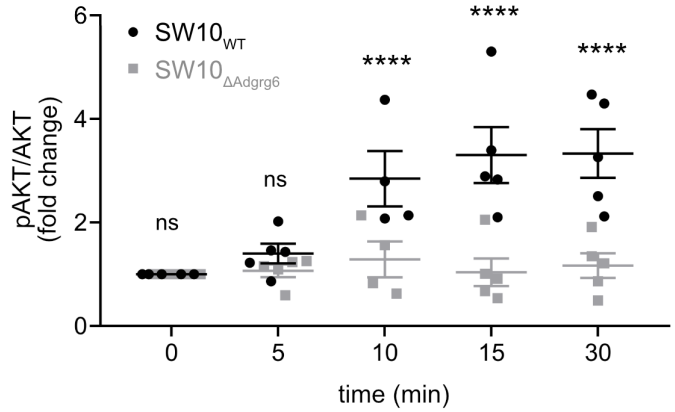

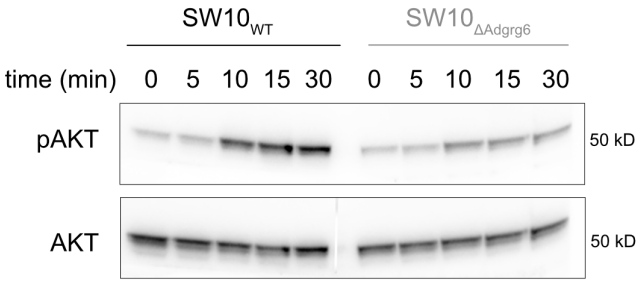

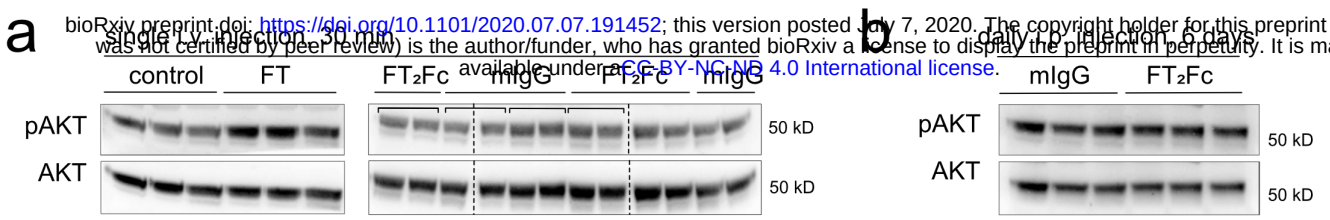

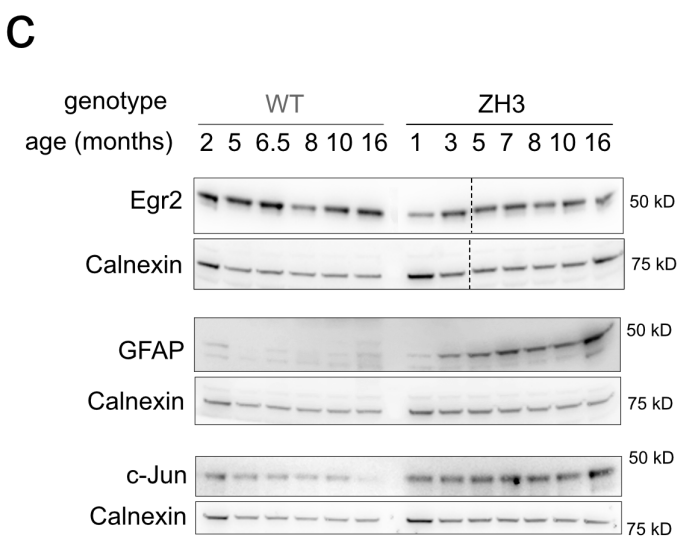

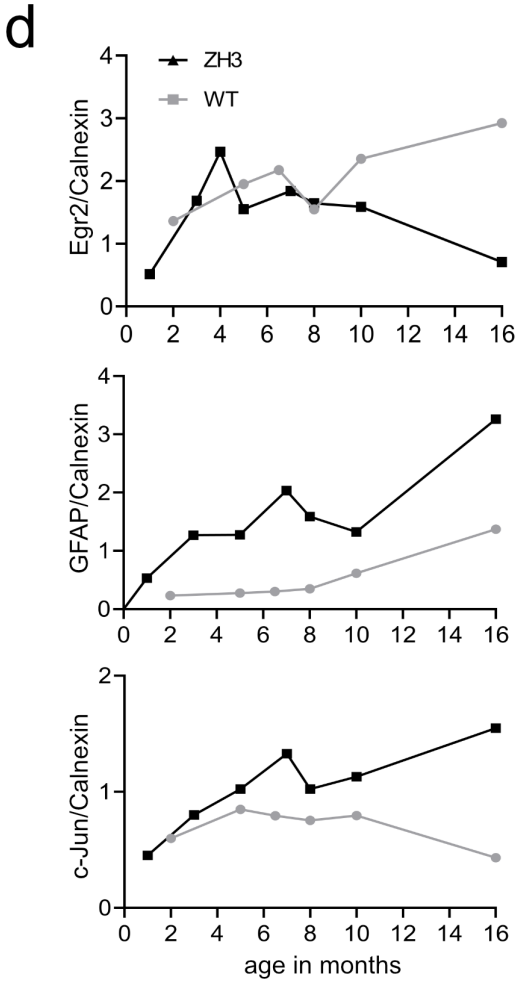

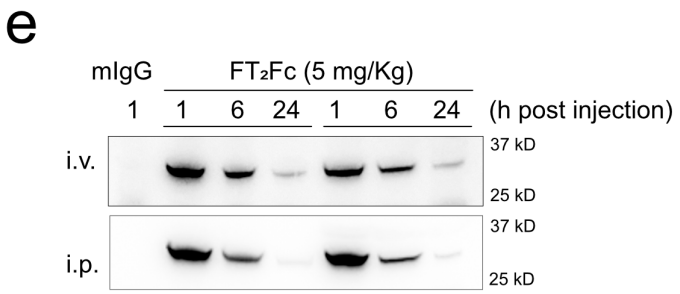

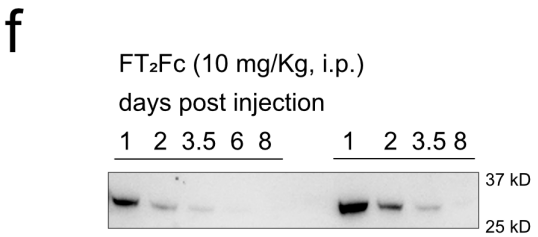

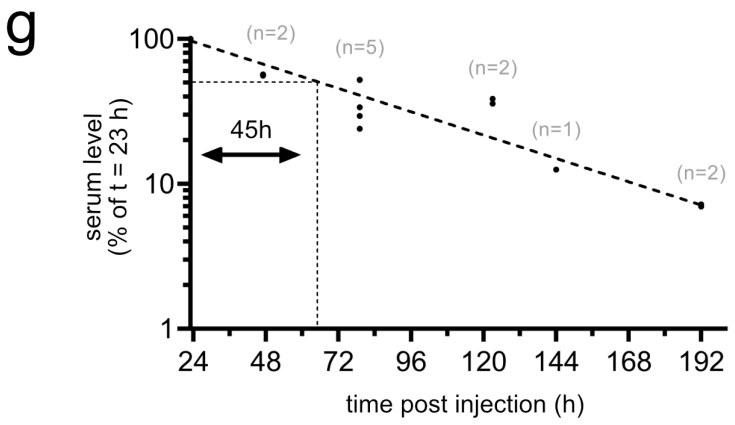

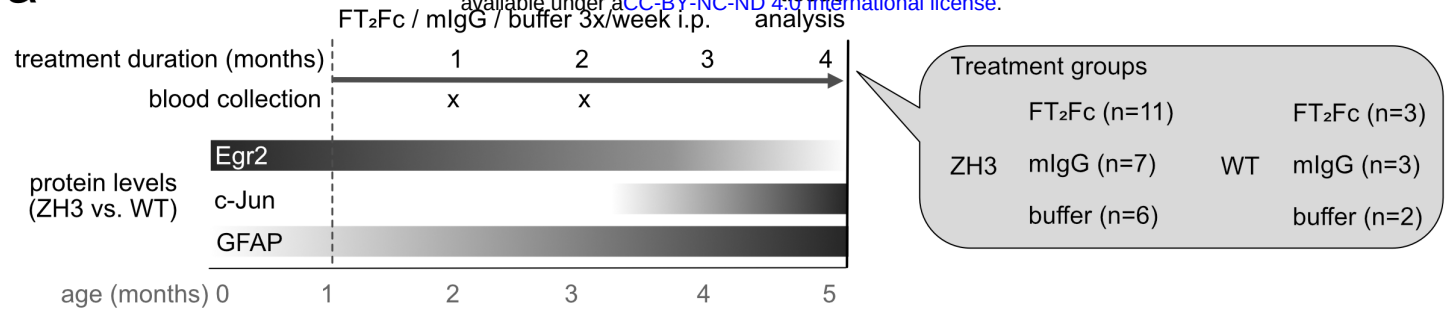

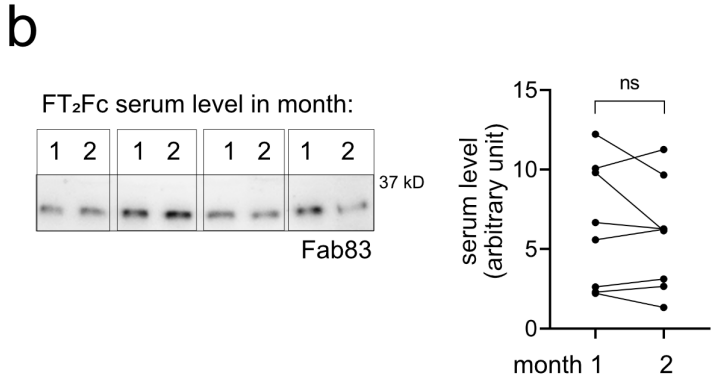

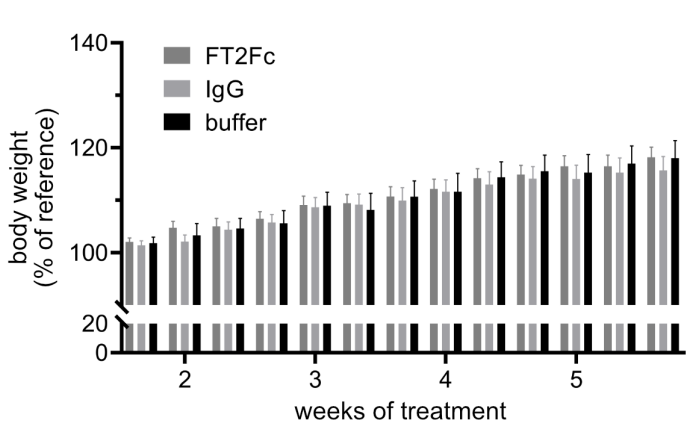

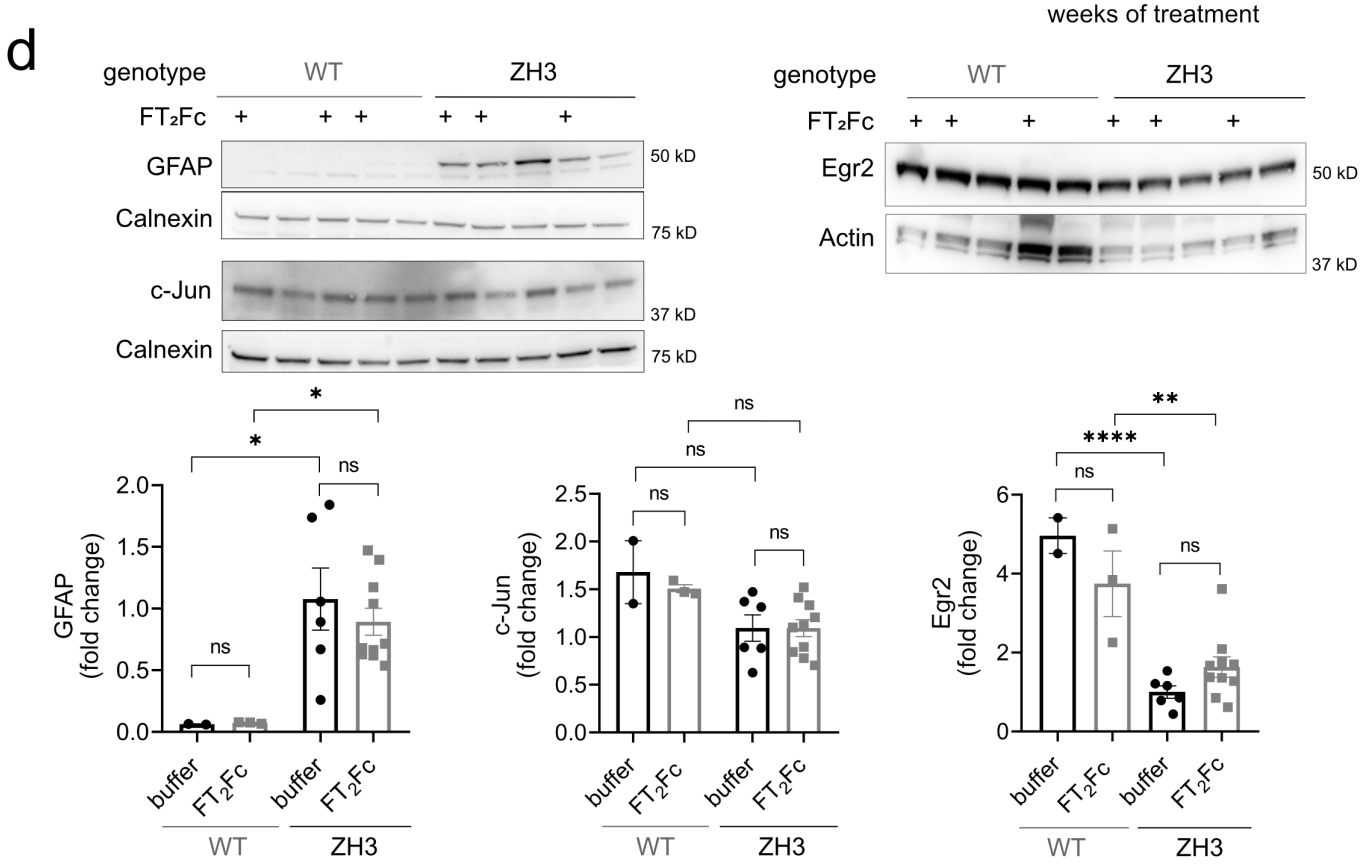

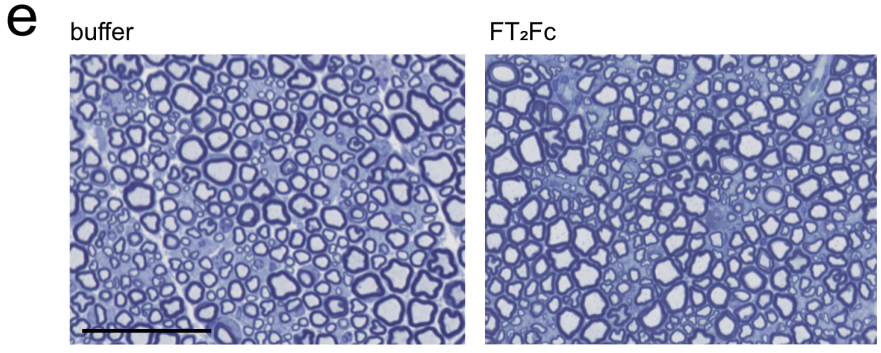

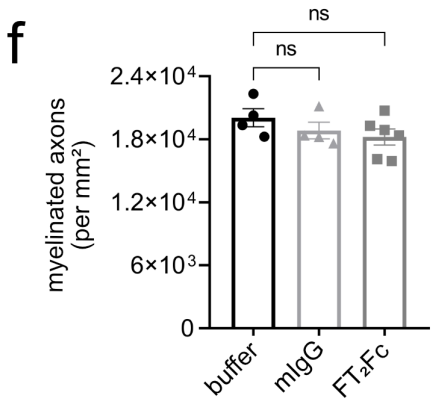

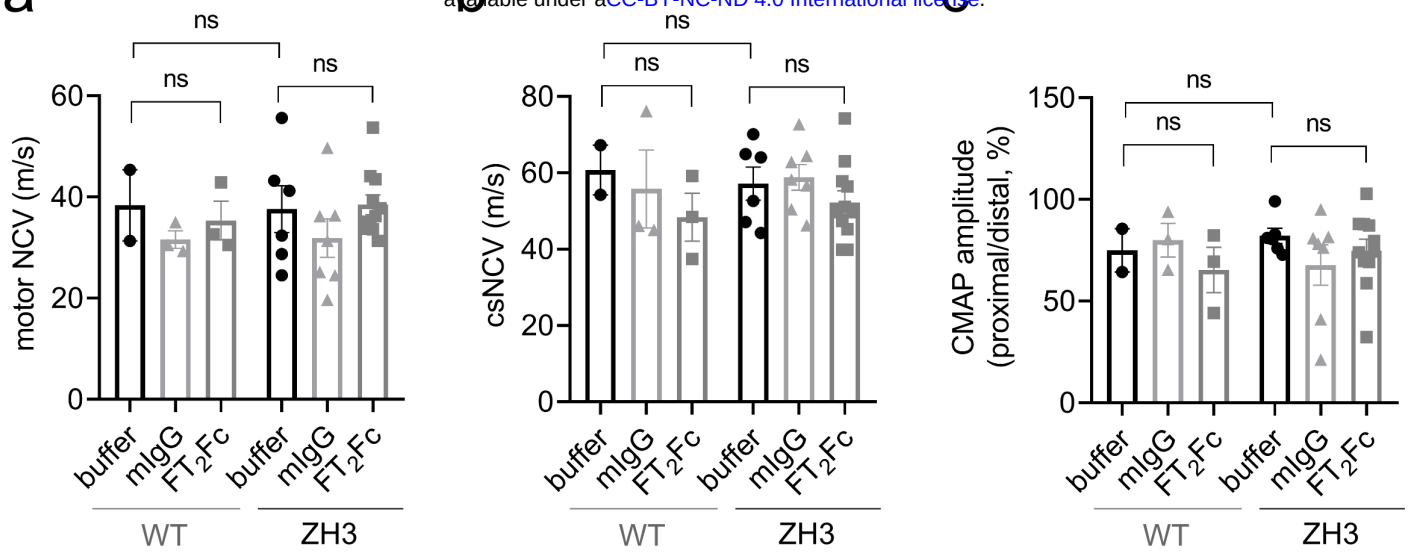

a

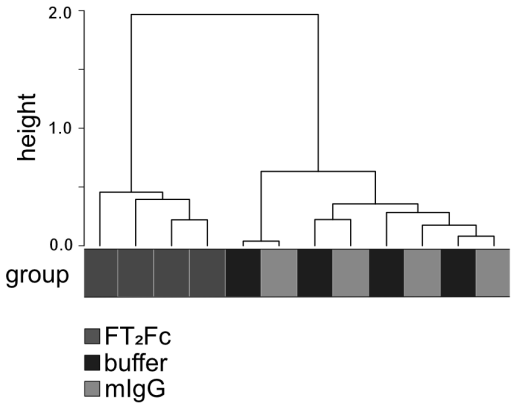

b

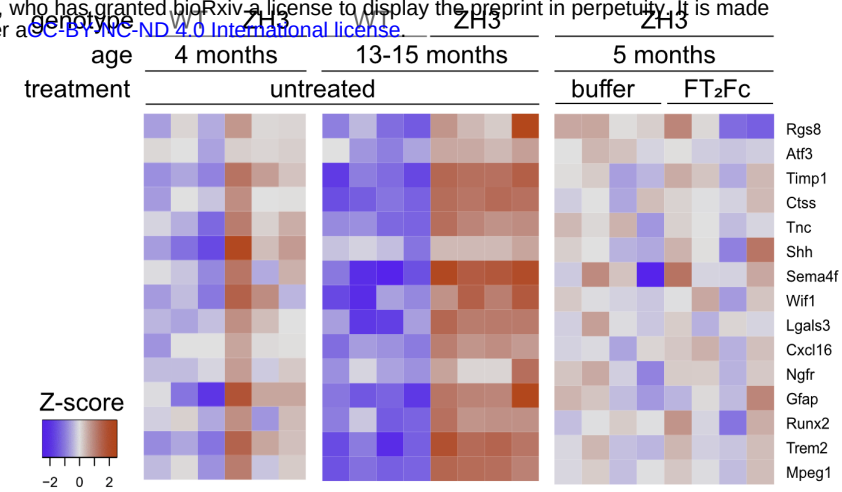

c

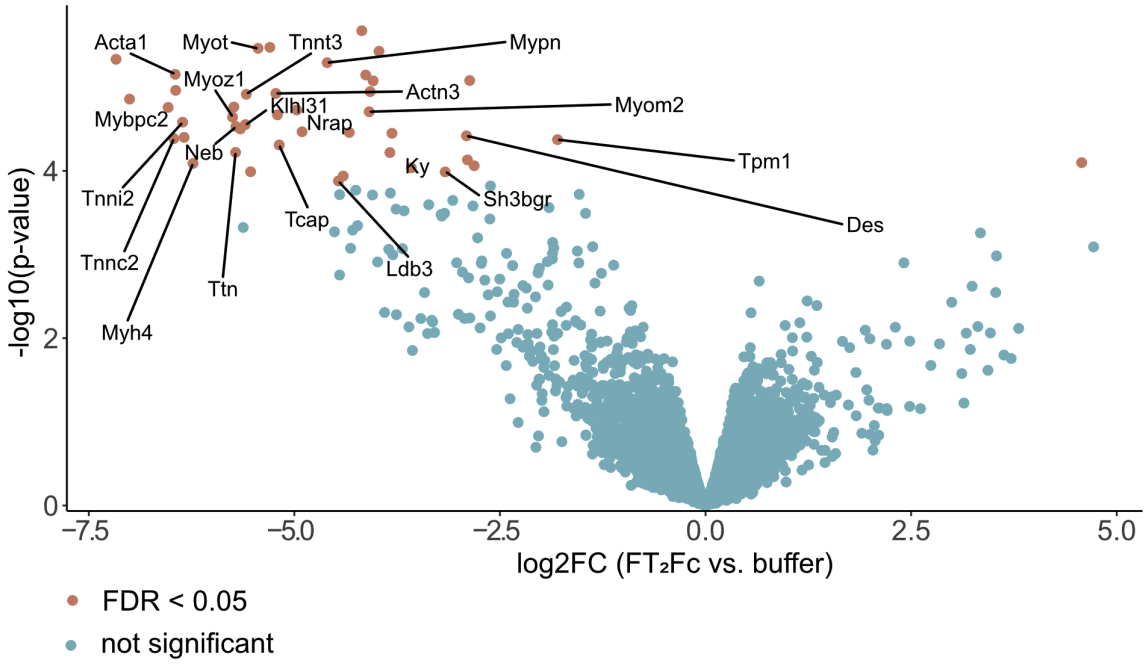

a

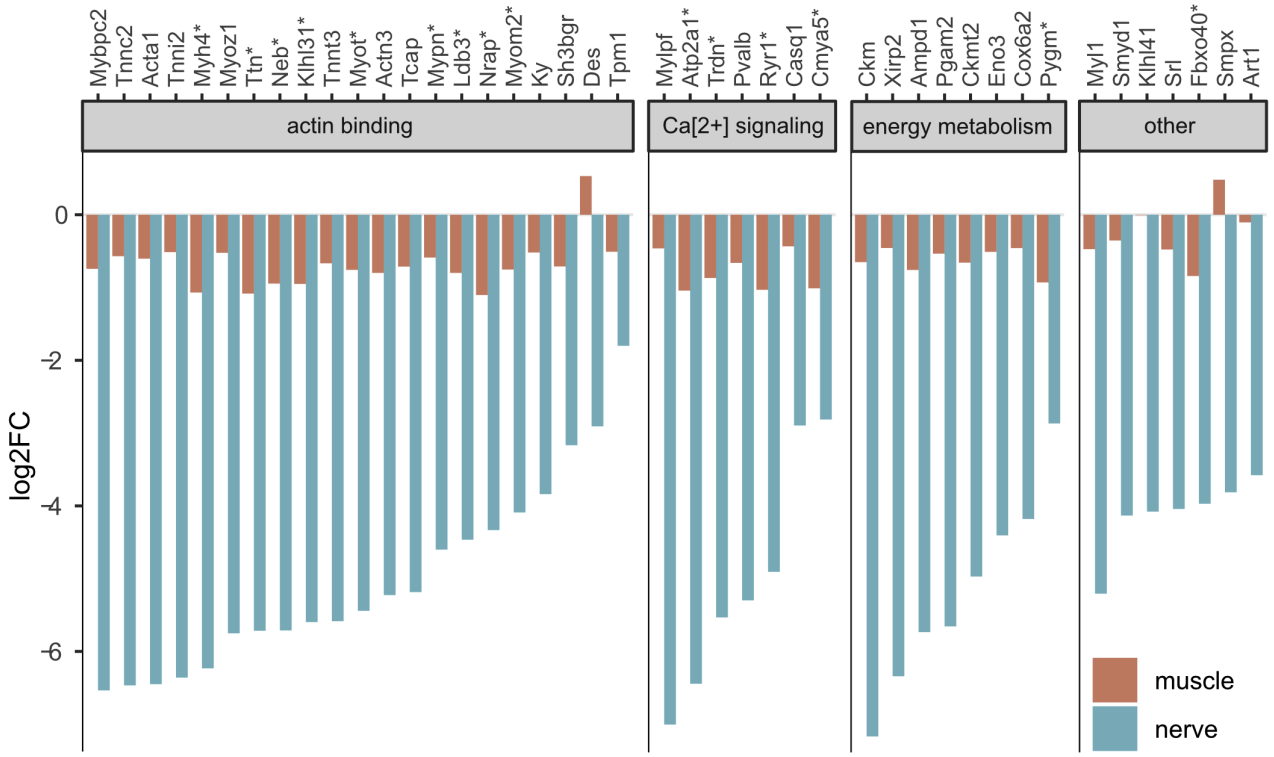

b

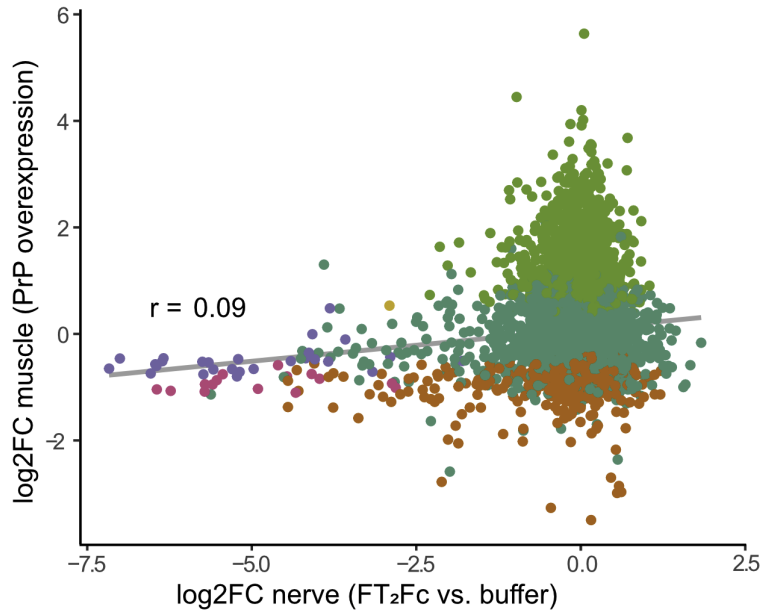

c